DOI: 10.1002/cssc.201402862

Synthesis of One-Dimensional Copper Sulfide Nanorods as High-Performance Anode in Lithium Ion Batteries

Xue Li,[a] Xinyi He,[a] Chunmei Shi,[a] Bo Liu,[a] Yiyong Zhang,[a] Shunqing Wu,[b] Zizong Zhu,[b] and Jinbao Zhao*[a]

Nanorod-like CuS and Cu_2S have been fabricated by a hydrothermal approach without using any surfactant and template. The electrochemical behavior of CuS and Cu_2S nanorod anodes for lithium-ion batteries reveal that they exhibit stable lithium-ion insertion/extraction reversibility and outstanding rate capability. Both of the electrodes exhibit excellent capacity retentions irrespective of the rate used, even at a high current density of 3200 mA g^{-1}. More than 370 mAh g^{-1} can be retained for the CuS electrode and 260 mAh g^{-1} for the Cu_2S electrode at the high current rate. After 100 cycles at 100 mA g^{-1}, the obtained CuS and Cu_2S electrodes show discharge capacities of 472 and 313 mAh g^{-1} with retentions of 92% and 96%, respectively. Together with the simplicity of fabrication and good electrochemical properties, CuS and Cu_2S nanorods are promising anode materials for practical use the next-generation lithium-ion batteries.

Introduction

Lithium ion batteries (LIBs) are currently the dominant power source for a range of portable electronic devices due to its long cycle life and high energy density.[1–3] However, the deployment of large-scale LIBs for application in hybrid electric vehicles (HEVs) is significantly hindered by several major technological barriers, including insufficient cycle life, poor charge–discharge rate capability, and intrinsically poor safety characteristics.[4,5] Therefore, the search for electrode materials to meet these requirements is critical for large-scale battery development.

As a new class of anode electrode materials for LIBs, metal sulfides are known to be promising materials for secondary lithium-metal batteries because of their high theoretical capacity.[6,7] Copper sulfides, in particular, have been attracting attention because of its advantages of high theoretical capacity, long and flat discharge voltage plateau, and good electrical conductivity.[8,9] However, they usually suffer from poor capacity retention upon cycling and/or poor rate capability, which is caused by the volume change during cycling, the instability of the carbonate-type electrolyte, and the loss of active material due to dissolution of sulfide species.[10–12] One generally accepted strategy to alleviate these problems is to prepare nanometer-sized materials with designed structure.[9,11,13]

One-dimensional (1D) nanostructures have attracted a considerable attention as it allows for better accommodation of volume change during repeated charge–discharge. Although a wide range of materials with various types of 1D nanostructures have been prepared by using different strategies,[14–19] it remains a challenge to synthesize 1D nanostructures of metal sulfides with isotropic crystal structure.

Herein, nanorod-like CuS and Cu_2S hierarchical structures have been fabricated by a hydrothermal approach without using any surfactant and template. Compared with conventional hydrothermal synthesis,[20–23] we can prepare different components of copper sulfides with high crystallinity and purity by our proposed method. As anodes for rechargeable LIBs, the synthesized copper sulfides with hierarchical nanostructures exhibit outstanding cycling stability and high rate performance.

Results and Discussion

The XRD patterns of the as-prepared CuS and Cu_2S nanorods in Figure 1 show good crystallization. All diffraction peaks in the left pattern can be indexed to the orthorhombic cell of CuS with lattice constants $a = 0.376$ nm, $b = 0.656$ nm, and $c = 1.624$ nm using values from literature (JCPDS: 03-065-7111). The right pattern can be indexed as the orthorhombic cell of Cu_2S with lattice constants $a = 1.350$ nm, $b = 2.732$ nm, and $c = 1.185$ nm, consistent with the values in the literature (JCPDS: 00-003-1071). For both samples, diffraction peaks of impurities could not be observed.

SEM images of CuS and Cu_2S nanorods are shown in Figure 2. Both of the samples prepared using the hydrothermal synthesis method exhibit a rod-like morphology. The rod diameters for the two samples are roughly 100–200 nm. Compared

[a] X. Li, X. He, C. Shi, B. Liu, Y. Zhang, J. Zhao
State Key Laboratory of Physical Chemistry of Solid Surfaces
Department of Chemistry
College of Chemistry and Chemical Engineering
Xiamen University
Xiamen 361005 (PR China)

[b] S. Wu, Z. Zhu
Department of Physics
Xiamen University
Xiamen 361005 (PR China)

Supporting Information for this article is available on the WWW under http://dx.doi.org/10.1002/cssc.201402862.

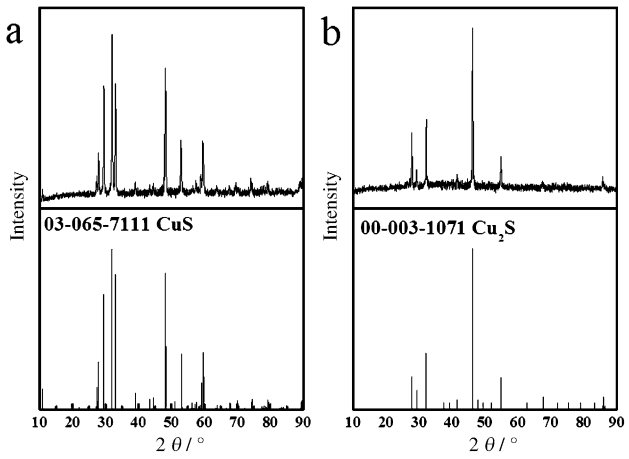

Figure 1. XRD patterns of the a) CuS and b) Cu_2S nanorods compared with the respective standard material cards.

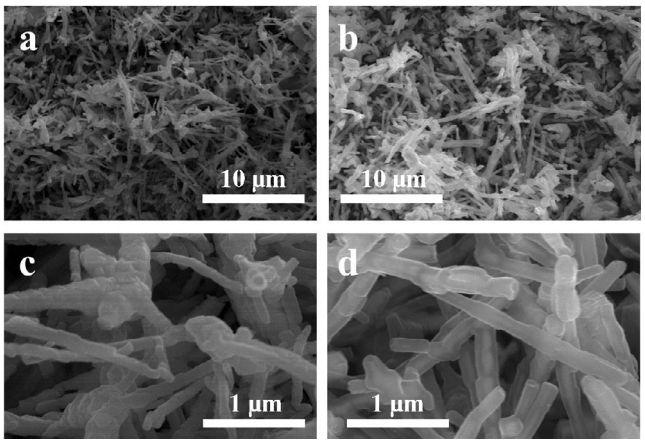

Figure 2. SEM images of the as-prepared CuS (a, c) and Cu_2S (b, d) nanorods at different magnifications.

with the CuS nanorods, the Cu_2S nanorods had larger diameters and a core–shell structure.

To further reveal the microstructure of the rod-like samples, TEM images were recorded (Figures 3a and 4a, b). The selected area electron diffraction (SAED) pattern (Figure 3b) corresponding to a flat-lying nanorod (Figure 3a) shows a regular hexagonal array of diffraction spots, corresponding to the basal plane of its structure, with the electron beam in the [001] direction. This pattern corresponds to a single crystal of covellite-like CuS.[24] The energy-dispersive X-ray (EDX) spectrum of the CuS nanorods is shown in Figure 3c. Peaks attributable to carbon, sulfur, and copper can be observed. The atomic ratio of S/Cu is 0.87, with the redundant copper and the small amounts of carbon maybe stemming from the copper wire mesh.

As shown in Figure 4a, the thickness of the Cu_2S nanorod core and shell are about 100 and 40 nm, respectively. The high-resolution (HR)TEM image in Figure 4b reveals that the Cu_2S in the shell is amorphous. This is different to the shell structure, in which the side face of the core structure corresponds to the {001} plane[25] with good crystallization.

To identify the composition of the core–shell structure, EDX spectra were obtained from the respective areas in Figure 4a. Peaks attributable to carbon, oxygen, sulfur and copper, with an atomic ratio of S/Cu of 3.84 in the shell and of 0.47 in the core. It illustrates that the shell structure is rich in sulfur and that the composition of the core is close to that of Cu_2S.

Figure 5 shows the comparison of the electrochemical performance of the CuS and Cu_2S nanorods. Both of the samples exhibit excellent cycling stability: for the CuS electrode, a capacity of 472 mAh g^{-1} could be retained after 100 cycles (corresponding to a capacity retention of 92%). In the case of the Cu_2S electrode, it delivered 313 mAh g^{-1} after 100 cycles with a high capacity retention of 96%.

For gaining further insight into the electrochemical performance, a comparison of the voltage profiles of the prepared CuS and Cu_2S electrodes were recorded (Figure 5c and d). Both samples also show the initial coulombic efficiency (94% for CuS and 93% for Cu_2S) and high initial discharge capacities (547 mAh g^{-1} for CuS and 350 mAh g^{-1} for Cu_2S), suggesting that both are optimal for practical usage as electrode materials. For the CuS electrode, two clear voltage plateaus at 2.1 and 1.7 V were observed in the first five cycles. After the 10th cycle, there is only one voltage plateau at 1.7 V. The mechanism of lithium uptake in CuS electrode is based on the following Reactions (1) and (2):[12,26,27]

$$CuS + Li \rightarrow 0.5\,Cu_2S + 0.5\,Li_2S \quad (1)$$

$$0.5\,Cu_2S + Li \rightarrow Cu + 0.5\,Li_2S \quad (2)$$

which give rise to a theoretical capacity of 560 mAh g^{-1}. The first discharge step with a short voltage plateau at 2.1 V is associated with Reaction (1), and the long voltage plateau at 1.7 V is related to Reaction (2). To confirm that Reaction (1) occurs, ex situ XRD analysis was performed at the short voltage plateau (2.1 V): CuS has been completely transformed into Cu_2S (see Figure S1 in the Supporting Information). For the Cu_2S electrode, there is only one long voltage plateau at 1.7 V, which corresponds to Reaction (2) and a theoretical capacity of 336 mAh g^{-1}. It is remarkable that the discharge curve of the Cu_2S shows a long, flat voltage plateau, which ensures a constant power output and is, therefore, very important for the commercial use of power sources. It seems clear from the charge–discharge profiles, that there is a temporary potential plateau around 2.3 V in the initial charge process and that the temporary potential fades out more quickly in the Cu_2S electrode. According to data reported and our best knowledge, the unstable plateau may be due to the initial potential barrier and can be improved by inducing polysulfide phase.[28] Because the lithium bonding environment in Li_2S is more like that in polysulfide than in the pure electrolyte, the charge-transfer process occurs more easily between Li_2S and the polysulfide during charging. Hence, the potential barrier can be eliminated faster in Cu_2S than in CuS electrode.

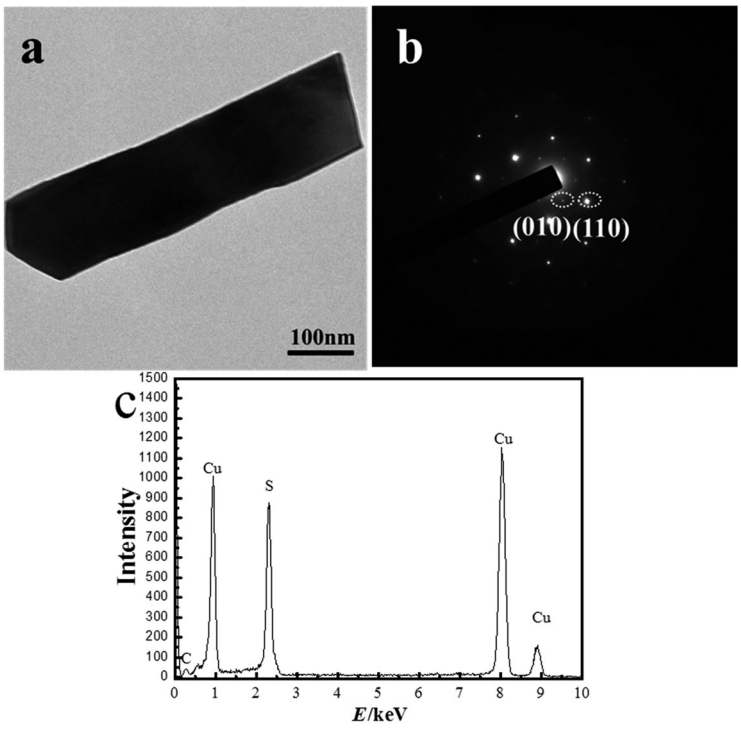

Figure 3. a) TEM image, b) SAED pattern, and c) EDX spectrum of the CuS nanorods.

The comparison of the rate capabilities between the CuS and Cu_2S electrodes at different current rates is shown in Figure 5e and f. As observed from these data, all samples showed excellent capacity retention irrespective of the rate used. Interestingly, more than 370 mAh g^{-1} can be retained for the CuS electrode and 260 mAh g^{-1} for the Cu_2S electrode even at a high current rate (3200 mA g^{-1}).

To gain more information of electrode kinetics, electrochemical impendence spectroscopy (EIS) was performed on the CuS and Cu_2S half cells (Figure 6). Both EIS diagrams are composed of a depressed semicircle at high frequencies and a spike at low frequencies. The high-frequency semicircle is related to the charge-transfer resistance whereas the spike at the low frequency end is an indication of Warburg impedance of long-range Li-ion diffusion.[29] For the two electrodes, there is a smaller Warburg impendence in the long voltage plateau (half discharged–charged state) and a bigger charge-transfer impendence in the fully charged state. These changes in impedance may be due to the formation of metallic copper with high conductivity and Li_2S with good ionic conductivity. Clearly, the tilt angle is around 45° in the Warburg region for the half discharged–charged state, which indicates that the electrochemical process is controlled by mass transfer.[30] It is interesting that the tilt angle is similar at the same degree of charge–discharge for the Cu_xS ($x=1$, 2) nanorod electrodes, suggesting outstanding electrochemical reversibility. Compared with CuS, the Cu_2S electrodes display a smaller impedance under the same conditions, which indicates that the electrochemical activity for Cu_2S is superior to that of the CuS anodes.

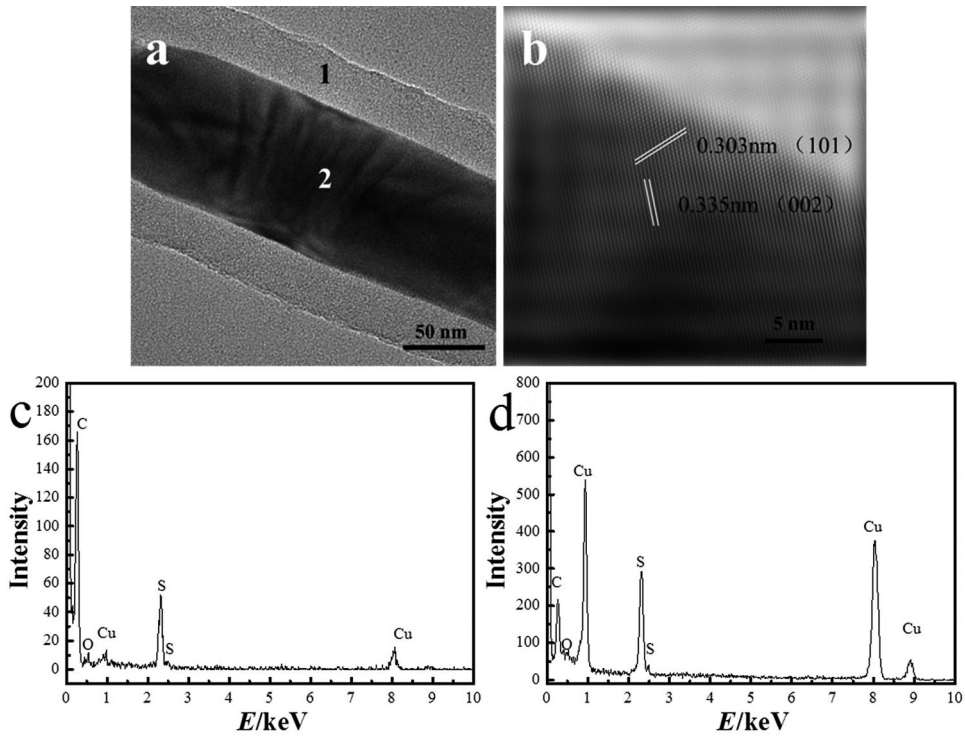

Figure 4. a) TEM image of a Cu_2S nanorod, b) HRTEM image of the selected area 2 in (a), c) the corresponding EDX spectrum from selected area 1 in (a), d) the corresponding EDX spectra from selected area 1 in (a).

Considering the relationship between crystal structure change and electrochemical mechanism, we used the Vienna ab initio simulation package (VASP) to evaluate the electrochemical process. The simulation results are shown in Table 1, and the schematic diagram about the electrochemical mechanism is displayed in Figure 7 (in Figure 7, the yellow balls represent as sulfur, the blue balls represent as copper and the green balls represent as lithium). It is worth noting that Cu_2S and Li_2S have the similar crystal structure: (1) the space groups are both face-centered cubic, (2) have similar lattice parameters (CuS: 5.711 Å, Cu_2S: 5.575 Å), and (3) have similar cell volume (CuS: 182.29 $Å^3$, Cu_2S: 173.32 $Å^3$). We also calculated the theoretic volume change of the prepared

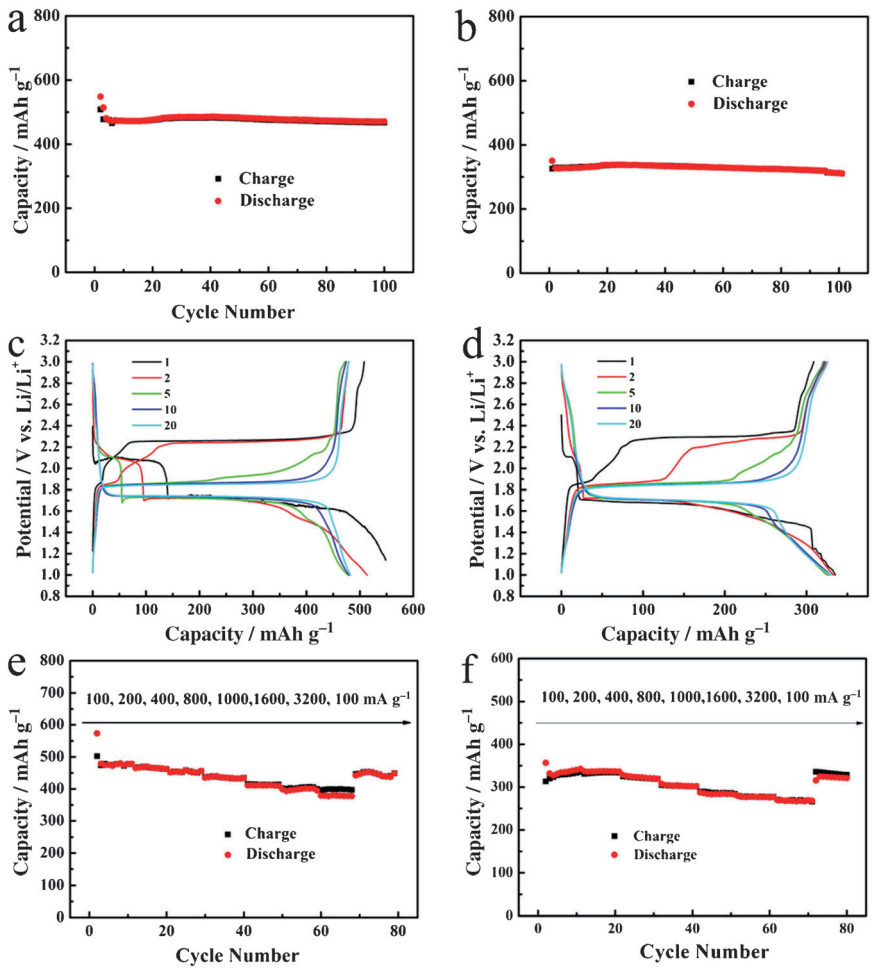

Figure 5. Cycle performance for a) CuS and b) Cu_2S nanorods for 100 cycles at a current density of 100 mA g^{-1}. Charge–discharge profiles of c) CuS and d) Cu_2S nanorods. Rate capabilities of e) CuS and f) Cu_2S nanorods at different current densities.

Table 1. Crystal-structure simulation results of CuS and Cu_2S obtained by using the VASP method.

Elements	Lattice parameter *a* [Å]	Space group	Cell volume [Å^3]	Number in formula
Li	3.44	Im$\bar{3}$m (fcc)	40.69	2
Cu	3.63	Fm$\bar{3}$m (fcc)	47.98	4
Li_2S	5.71	Fm$\bar{3}$m (fcc)	186.29	4
Cu_2S	5.58	Fm$\bar{3}$m (fcc)	173.32	4
CuS	3.81	monoclinic	414.22	12

materials. According to Reaction (1) discussed above, there is a volume change of approximately 0.054 cm^3 g^{-1} for CuS and 0.0395 cm^3 g^{-1} for Cu_2S. As shown in Figure 7, at 2.1 V the monoclinic CuS firstly transforms to face-centered cubic Cu_2S and then reacts with lithium in the Cu_2S form. In short, the Cu_2S and Li_2S structure present exactly the similar crystal structure, which enables the material to be insert and remove Li highly reversible during the charge–discharge process and thus show good rate performance.

Conclusions

One-dimensional Cu_xS ($x=1$, 2) nanorods have been prepared by using a template- and surfactant-free solvent thermal method. The superiority of this approach lies in the fact that the composition of highly crystalline Cu_xS can be precisely controlled. An electrode using this synthetic Cu_xS exhibited a good rate capability and high electrochemical stability for lithium storage. At a current density of 100 mA g^{-1}, the CuS and Cu_2S electrodes showed discharge capacities of 472 and 313 mAh g^{-1} with retentions of 92% and 96% after 100 cycles, respectively. Both of the electrodes showed excellent capacity retentions irrespective of the rate used. Even when discharging at a current density as high as 3200 mA g^{-1}, more than 370 mAh g^{-1} could be retained for the CuS electrode and 260 mAh g^{-1} for the Cu_2S electrode. The theoretical calculation results obtained by using VASP also indicate that Cu_xS has outstanding electrochemical properties. Considering the improved performance and cost-effective synthesis, we believe that the solvothermal method could be applied to preparing metal sulfides and the as-prepared Cu_xS nanorods that might be suitable as negative electrodes for next-generation lithium-ion batteries.

Experimental Section

Synthesis: All chemical reagents of analytic grade purity were purchased from Shanghai Chemical Co. Ltd. and were used without further purification. In this paper, we reported the synthesis of hierarchical self-supported micropatterns of Cu_xS by the reaction of $CuSO_4{\cdot}5H_2O$ and dimethyl sulfoxide (DMSO) at a suitable concentration, in which DMSO played multiple roles: a solvent, a sulfur source, and a reducing agent. The details of the synthesis are shown below.

CuS: In a typical synthesis, $CuSO_4{\cdot}5H_2O$ (0.0075 mol) was added to DMSO (80 mL) to form a clear green solution under constant stirring for 10 min. This solution was placed in a Teflon-sealed autoclave (volume 100 mL), which was maintained at 180 °C for 6 h. Then the solution was filtered and the obtained solid contents were dried under vacuum at 80 °C for 10 h after several cycles of centrifugation and dispersion using deionized water.

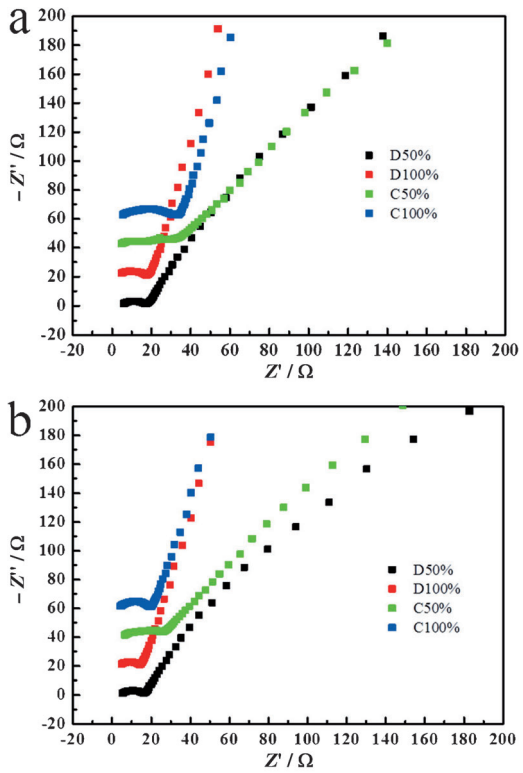

Figure 6. Nyquist plots of the a) CuS and b) Cu_2S electrodes at different states of charge and discharge (half discharged–charged state referred to as D/C 50% and fully discharged–charged state referred to as D/C 100%) in the 10th cycle.

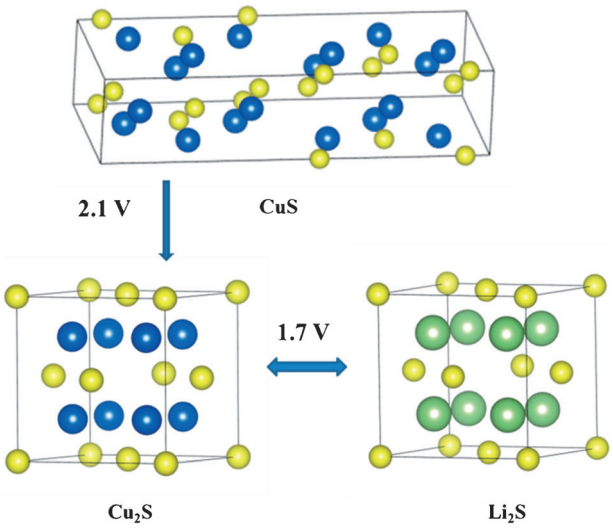

Figure 7. Brief schematic diagram of the electrochemical charge–discharge mechanism of CuS and Cu_2S anodes.

Cu_2S: $CuSO_4 \cdot 5H_2O$ (0.02 mol) was added to DMSO (40 mL) to form a clear green solution under constant stirring for 10 min. This solution was placed in a Teflon-sealed autoclave (volume 100 mL), which was maintained at 180 °C for 6 h. Then the solution was filtered, and the obtained solid contents were dried under vacuum at 80 °C for 10 h after several cycles of centrifugation and dispersion using deionized water.

Characterization: The XRD patterns were recorded using a Philips X'pert Pro Super X-ray diffract meter and CuK_α radiation. The morphologies of the as-prepared materials were characterized by using a field-emission SEM (LEO 1530, HITACHI S-4800) and a HRTEM (JEM-2100).

Electrochemical characterization: Electrochemical evaluations were performed by galvanostatically cycling the electrodes constructed by using as-prepared Cu_xS ($x = 1$, 2) samples in a CR2016-type coin cell. The working electrodes were formed by casting a slurry with a composition of 70 wt% active materials, 20 wt% carbon black, and 10 wt% polyvinylidene fluorides (PVDF), which was dissolved in *N*-methylpyrrolidinone (NMP) prior to the experiment, onto a copper current collector foil. Afterwards, the electrodes were dried under vacuum at 110 °C for 12 h. The cells were assembled using the prepared electrodes as anodes and lithium metal as cathode. The electrolyte was prepared by adding lithium bis(trifluoromethanesulfonyl)imide (LiTFSI; 1 M) salt to a mixture of 1,2-dimethoxyethane (DME) and 1,3-dioxolane (DOL) at a 1:1 volume ratio. All assembly processes of the test cells were carried out in an argon-filled glove box. Galvanostatic charge–discharge experiments were performed at different current densities between 1.0 and 3.0 V (vs. Li/Li^+) using a CT2001A cell test instrument (LAND Electronic Co.). The EIS of the Cu_xS electrodes discharged at different voltages were recorded by using an Autolab PGSTAT 101 cell test instrument in the frequency range of 10 mHz–100 kHz by using two-electrode coin cells with Li metal as the counter electrode.

Caculation procedure: All the calculations were performed by using the VASP package[31, 32, 25], the code of which is based on the first-principles density-functional theory(DFT).[33] The electronic exchange correlation energy was modeled using the Perdew–Burke--Ernzerhof (PBE) function within the generalized gradient approximation (GGA).[34] The wave functions were expanded by means of plane waves using a kinetic energy cutoff of 350 eV. All atomic configurations were fully relaxed until the Hellmann–Feynman forces on all the atoms were smaller than 0.01 eV $Å^{-1}$. The Brillouin zone integrations were approximated by using a special *k*-point sampling of the Monkhorst–Pack scheme. We used different *k*-point setting methods according to the special crystal structure because different crystal structures were involved in our work.

Acknowledgements

The authors gratefully acknowledge financial support from National Natural Science Foundation of China (21273185and 21321062) and the National Fund for Fostering Talents of Basic Science (Grant No. J1310024). The authors also wish to express thanks Dr. Peng Zhang of Xiamen University for their valuable suggestions.

Keywords: anode · batteries · copper sulfide · high performance · lithium

[1] T. Ohzuku, A. Ueda, N. Yamamoto, *J. Electrochem. Soc.* **1995**, *142*, 1431–1435.
[2] M. Armand, J. M. Tarascon, *Nature* **2008**, *451*, 652–657.
[3] D. J. Lee, M. Agostini, J. W. Park, Y. K. Sun, J. Hassoun, B. Scrosati, *ChemSusChem* **2013**, *6*, 2245–2248.
[4] L. F. Shen, H. S. Li, E. Uchaker, X. G. Zhang, G. Z. Cao, *Nano Lett.* **2012**, *12*, 5673–5678.

[5] E. Kang, Y. S. Jung, A. S. Cavanagh, G. H. Kim, S. M. George, A. C. Dillon, J. K. Kim, J. Lee, *Adv. Funct. Mater.* **2011**, *21*, 2430 – 2438.
[6] J. Z. Wang, S. L. Chou, S. Y. Chew, J. Z. Sun, M. Forsyth, D. R. Macfarlane, H. K. Liu, *Solid State Ionics* **2008**, *179*, 2379 – 2382.
[7] J. Zhao Wang, L. Lu, M. Lotya, J. N. Coleman, S. L. Chou, H. K. Liu, A. I. Minett, J. Chen, *Adv. Energy Mater.* **2013**, *3*, 798 – 805.
[8] Y. Chen, C. Davoisne, J. Tarascon, C. Guery, *J. Mater. Chem.* **2012**, *22*, 5295 – 5299.
[9] Y. Han, Y. Wang, W. Gao, *Powder Technol.* **2011**, *212*, 64 – 68.
[10] S. C. Han, M. S. Song, H. Lee, H. S. Kim, H. J. Ahn, J. Y. Lee, *J. Electrochem. Soc.* **2003**, *150*, A889 – A893.
[11] Y. Wang, X. Zhang, P. Chen, H. Liao, *Electrochim. Acta* **2012**, *80*, 264 – 268.
[12] B. Jache, B. Mogwitz, F. Klein, P. Adelhelm, *J. Power Sources* **2014**, *247*, 703 – 711.
[13] F. Bonino, M. Lazzari, B. Rivolta, B. Scrosati, *J. Electrochem. Soc.* **1984**, *131*, 1498 – 1502.
[14] X. W. Lou, D. Deng, J. Y. Lee, J. Feng, L. A. Archer, *Adv. Mater.* **2008**, *20*, 258 – 262.
[15] Z. Liu, D. Zhang, S. Han, C. Li, B. Lei, W. Lu, J. Fang, C. Zhou, *J. Am. Chem. Soc.* **2005**, *127*, 6 – 7.
[16] H. J. Fan, M. Knez, R. Scholz, K. Nielsch, E. Pippe, D. Hesse, M. Zacharias, U. Gosele, *Nat. Mater.* **2006**, *5*, 627 – 631.
[17] J. Goldberger, R. He, Y. F. Zhang, S. Lee, H. Yan, H. J. Cho, P. D. Yang, *Nature* **2003**, *422*, 599 – 602.
[18] Q. Lu, F. Gao, D. Zhao, *Nano Lett.* **2002**, *2*, 725 – 728.
[19] C. H. Lai, K. W. Huang, J. H. Chenq, C. Y. Lee, B. J. Hwanq, L. J. Chen, *J. Mater. Chem.* **2010**, *20*, 6638 – 6645.
[20] P. Roy, SK. Srivastava, *Matel Lett.* **2007**, *61*, 1693 – 1697.
[21] X. B. Wang, C. Q. Xu, Z. C. Zhang, *Matel Lett.* **2006**, *60*, 345 – 348.
[22] M. B. Sigman, A. Ghezelbash, A. E. Saunders, F. Lee, B. A. Korgel, *J. Am. Chem. Soc.* **2003**, *125*, 16050 – 16057.
[23] W. X. Zhang, X. G. Wen, S. H. Yang, *Langmuir* **2003**, *19*, 4420 – 4426.
[24] T. Thongtem, C. Pilapong, S. Thongtem, *Matel Lett.* **2010**, *64*, 111 – 114.
[25] Z. Zhuang, Q. Peng, B. Zhang, Y. Li, *J. Am. Chem. Soc.* **2008**, *130*, 10482 – 10483.
[26] A. Débart, L. Dupont, R. Patrice, J. M. Tarascon, *Solid State Sci.* **2006**, *8*, 640 – 651.
[27] J. S. Chung, H. J. Sohu, *J. Power Sources* **2002**, *108*, 226 – 231.
[28] Y. Yang, G. Y. Zheng, S. Misra, J. Nelson, M. F. Toney, Y. Cui, *J. Am. Chem. Soc.* **2012**, *134*, 15387 – 15394.
[29] N. Schweikert, H. Hahn, S. Indris, *Phys. Chem. Chem. Phys.* **2011**, *13*, 6234 – 6240.
[30] A. K. Hjelm, G. Lindbergh, *Electrochim. Acta* **2002**, *47*, 1747 – 1759.
[31] G. Kresse, J. Furthmüller, *Comput. Mater. Sci.* **1996**, *6*, 15 – 50.
[32] G. Kresse, J. Furthmüller, *Phys. Rev. B* **1996**, *54*, 11169 – 11186.
[33] J. P. Perdew, J. A. Chevary, S. H. Vosko, K. A. Jackson, M. R. Pederson, D. J. Singh, C. Fiolhais, *Phys. Rev. B* **1992**, *46*, 6671 – 6687.
[34] H. Zhang, Y. H. Tang, J. Q. Shen, X. G. Xin, L. X. Cui, L. J. Chen, C. Y. Ouyang, S. Q. Shi, L. Q. Chen, *Appl. Phys. A* **2011**, *104*, 529 – 537.

Received: August 19, 2014
Revised: September 13, 2014
Published online on October 29, 2014